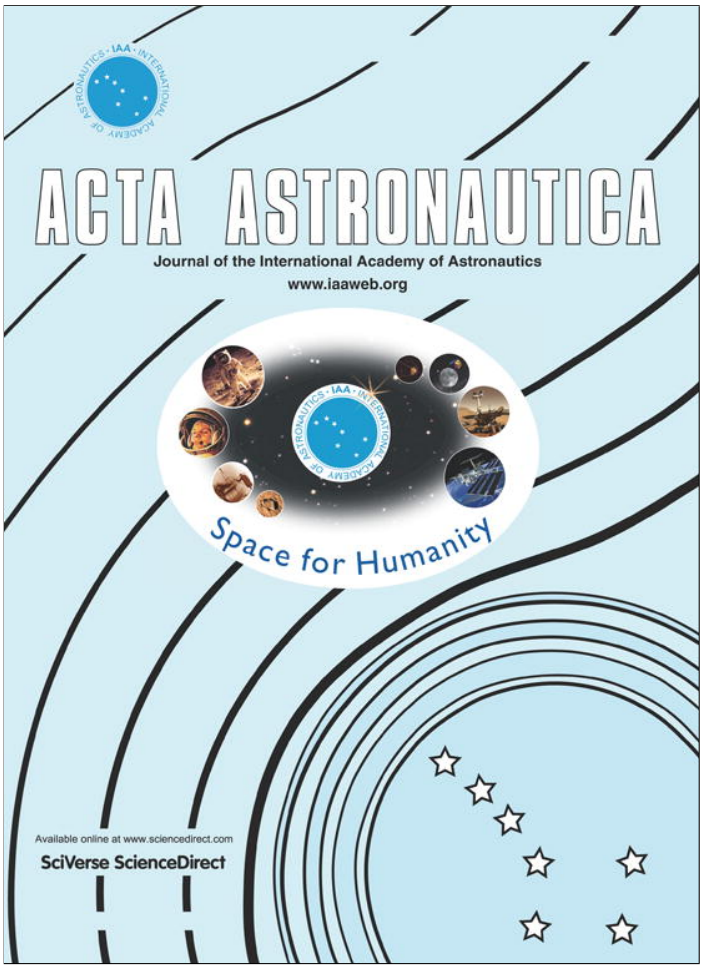

Acta Astronautica 89 (2013) 21–30

Contents lists available at SciVerse ScienceDirect

Acta Astronautica

journal homepage: www.elsevier.com/locate/actaastro

Periodic relative orbits of two spacecraft subject to differential gravity and electrostatic forcing

Drew R. Jones [a,*], Hanspeter Schaub [b]

[a] Aerospace Engineering and Engineering Mechanics Department, WRW Laboratories, The University of Texas at Austin, 210 E 24th St, Austin, TX 78712, United States

[b] Aerospace Engineering Sciences Department, Colorado Center for Astrodynamics Research, University of Colorado Boulder, Boulder, CO 80309-0431, United States

ARTICLE INFO

Article history:
Received 28 November 2012
Accepted 28 March 2013
Available online 10 April 2013

Keywords:
Coulomb formation flying
Periodic solutions
Relative motion
Nonlinear dynamical systems

ABSTRACT

Coulomb forces between charged close-flying satellites can be used for formation control, and constant electric potentials enable static equilibria solutions. In this work, open-loop time-varying potential functions, which produce periodic, two-craft, Coulomb formation motions are demonstrated for the first time. This is done in the rotating Hill-Frame, with linearized gravity, and craft position components assumed in the form of simple harmonic oscillators. Substitution of the oscillatory functions into the dynamics, further constrains these functions, and yields necessary potential histories, to produce the periodic flow. The assumed position functions, however, are not arbitrary, since the dynamical model restricts what oscillatory trajectories are allowed. Specifically, a Hill-Frame integral of motion is derived, and this is used to show certain candidate periodic functions to be inadmissible. The system dynamics are then linearized to expose stability properties of the solutions, and it is established that asymptotic stability is impossible for all orbit families. Finally, the degree of instability in the assumed motions, over free parameter ranges, is determined numerically via the Floquet multipliers of the associated full-cycle state-transition matrices.

1. Introduction

Spacecraft charge control was considered as early as 1966 by Cover, Knauer, and Maurer [1], who propose using electrostatic forces to inflate and maintain the shape of a large reflecting mesh. Coulomb formations introduced by King et al. [2,3], refer to the use of this concept in spacecraft formation flying, where the electric potential (or net charge) of each vehicle is actively controlled, to yield desired inter-craft forces. Close-proximity vehicles have many advantages over a single large spacecraft, including overall mass reduction, shape-changing ability, and multiple launches for deployment, assembly, and repair. Free-flying formations have applications in earth imaging, surveillance, and separated space-borne interferometry [2,4]. Initially, electric propulsion (EP) systems were proposed for controlling the relative craft motions; however, EP suffers from limited throttle-ability and the problem of thruster-plume impingement, where thruster ejecta may damage or impede neighboring craft [2]. In contrast, active charge control avoids thruster-plumes, has fast throttling (ms transitions), and can sustain a given force using less power and fuel than EP, yielding specific impulse (ISP) values as high as 10^{13} s [1,2]. Furthermore, active control of spacecraft charge was successfully executed during the SCATHA [5] and ATS [6] missions, and currently on the CLUSTER [7] mission. Other applications for electrostatic thrusting include advanced docking and rendezvous,

* Corresponding author.
E-mail addresses: drjones604@gmail.com, drjones604@utexas.edu (D.R. Jones).

0094-5765/$ - see front matter © 2013 IAA Published by Elsevier Ltd. All rights reserved.
http://dx.doi.org/10.1016/j.actaastro.2013.03.028

autonomous inspection, contact-less removal of hazardous material [8], and the deployment/retrieval of instruments [9].

Static Coulomb formation equilibria, in which constant potentials enable shapes that appear fixed with respect to their center-of-mass, are derived and analyzed extensively in the literature. These solutions are often referred to as 'virtual structures', since the separation distances (or ratios of the distances) are constant. Some derived static equilibrium includes 3-craft shapes in the absence of gravitational forces [10–12], 2-craft shapes under classical non-linear and circular-restricted 3-body (CRTBP) gravity [13], and 2- and 3-craft spinning configurations [14,15]. Berryman and Schaub [9,16], among others, have devoted much attention to those equilibria (up to N-craft) admitted in the rotating Hill-Frame model, with linearized gravity [2,17–19]. Berryman and Schaub conclude their work by stating that future investigations should be directed towards the derivation of dynamic and periodic Coulomb formations [9,16]. The first examples of such periodic Coulomb formation solutions are presented in this paper, and serve as natural and desired extensions of the static equilibria. These solutions are defined for two vehicles in the linearized gravity Hill-Frame model, where time-dependent charge histories produce assumed periodic motions in the craft positions. The periodic state functions cannot be assumed arbitrarily; however, because the set of admissible periodic flows is restricted by the underlying dynamics. An integral of motion, specific to the assumed dynamical model, is also derived in this research and is used to demonstrate certain candidate periodic functions as inadmissible. This scalar Hill-Frame integral of motion, is acquired from the fact that the system inertial angular momentum vector is conserved, in internally actuated formations (e.g. Coulomb formations). [20]

Various techniques are used to study stability properties associated with static Coulomb equilibria [14,15,19], and similar analyses are extended in this work, to periodic Coulomb formations. Specifically, the Lyapunov stability of the periodic solutions is studied using Floquet theory [21,22], and asymptotic stability is demonstrated to be impossible in the linearized systems. Moreover, the degree of instability is assessed via the maximum modulus Floquet multiplier (Monodramy matrix eigenvalue), for the parameterized orbit families. The Monodramy matrix is shown to share many analytical properties with those corresponding to periodic orbits, about libration points, in the CRTBP [23]. Feedback control and maneuvering of static equilibria cases are given much attention in the literature, and various authors exploit marginal modal stabilities to reduce station-keeping control effort [10,12,24–26]. Furthermore, Inampudi [13], and Jones and Schaub [27,28] develop methods to optimally transfer between certain static configurations, and each utilize zero-input stability properties inherent to those systems. The numerical stability analyses of periodic Coulomb motions established here, should prove useful in the eventual design of controllers, to maintain and maneuver these open-loop orbits.

2. Background and dynamical model

A conductive craft surface naturally exchanges ions and electrons with the plasma of space, and as a result assumes a non-zero electric potential ϕ (in Volts). When immersed in a plasma, an ideal vacuum potential is limited (or shielded) due to interactions with free particles and photons. The Debye length λ_d approximates this shielding, such that a charged particle at a distance $r > \lambda_d$ is unaffected by ϕ. Debye length is a measure of the time-dependent local plasma temperature and density, and experimental data are available in various regimes. For nominal conditions λ_d is on the order of 0.01 m at LEO, 200 m at GEO, and 10 m at Interplanetary [29,30]. However, the effective Debye length can be many times greater for ϕ much greater than the plasma energy [29,30], and in GEO λ_d can be larger for substantial periods of time [31]. A naturally resulting potential can be altered artificially, simply by ejecting electrons/ions into the surrounding plasma, using an electron-gun type device, and this has been demonstrated on multiple missions [5–7]. To do so, the device must have sufficient power to supply the desired voltage ϕ, while continuously emitting particles at a current (rate) greater than the incoming environmental current (which tends to drive ϕ to natural equilibrium).

In this work, all spacecraft are assumed spherical (radius R_{sc}), with perfectly conductive, outer surfaces of uniform charge density. Formations are considered in the GEO regime, such that $R_{sc} \ll \lambda_d$, making plasma shielding negligible over R_{sc}, and it is assumed that the capacitance of one craft is not impacted by its neighbors. These simplifications allow craft i net surface charge q_i to be accurately related to the potential ϕ_i, analytically via Eq. (1), where k_c is the Coulomb constant [30,17]:

$$\phi_i = k_c \frac{q_i}{R_{sc}} \tag{1}$$

Using Eq. (1), the q_i are considered as controls in this research, in substitution for the truly measurable/controllable parameters ϕ_i. Moreover, for the 2-craft system being addressed here, the product of the two charges $Q_{12} = q_1 q_2$, is also regarded as a fully controllable parameter.

2.1. General dynamical model

An Earth-centered inertial frame is denoted $\mathcal{N} : \{\hat{\imath}, \hat{\jmath}, \hat{k}\}$, and $\mathcal{H} : \{\hat{e}_R, \hat{e}_T, \hat{e}_N\}$ denotes the rotating Hill-Frame, which is centered at and rotates with a nominal center-of-mass (CM) orbit (assumed circular with semi-major-axis a_0). The axes correspond to $\hat{e}_R$ for radial, $\hat{e}_T$ for transverse (along-track), and $\hat{e}_N$ for normal (orbit-normal). Formation dynamics are considered in the Hill-Frame, as depicted in Fig. 1, where $\mathbf{R}_i$ is the craft i location in the $\mathcal{N}$ frame, $\mathbf{R}_{\rm cm}$ is the formation CM in the $\mathcal{N}$ frame, and $\mathbf{r}_i$ denotes craft i position relative to $\mathbf{R}_{\rm cm}$ (origin of the $\mathcal{H}$ frame). Eq. (2) shows how these position vectors are written in terms of each other, and Eq. (3) constraint on the $\mathbf{r}_i$ vectors is a consequence of the $\mathcal{H}$ frame definition. The linearized Clohessy–Wiltshire–Hill gravitational model [32], and a net Coulomb acceleration defined using the Debye–Hückel approximation [33] are assumed. Therefore, the Hill-Frame acceleration of craft i is defined by Eq. (4), where m_i and q_i denote craft i mass and net charge, respectively:

$$\mathbf{R}_i = \mathbf{R}_{\rm cm} + \mathbf{r}_i \tag{2}$$

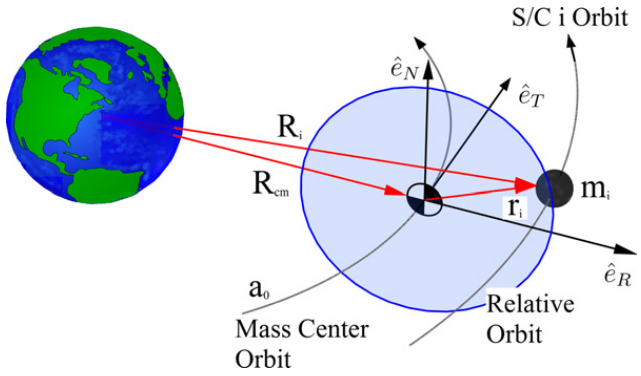

Fig. 1. Rotating Hill-Frame showing relative position vector $\mathbf{r}_i$

$$\sum_i m_i \mathbf{r}_i = 0 \quad \mathbf{r}_i = [x_i \; y_i \; z_i]^T \tag{3}$$

$$\ddot{\mathbf{r}}_i = \begin{bmatrix} 2\omega\dot{y}_i + 3\omega^2 x_i \\ -2\omega\dot{x}_i \\ -\omega^2 z_i \end{bmatrix} + \frac{k_c q_i}{m_i} \sum_{\substack{j \\ j\neq i}} \frac{q_j \left(1 + \frac{r_{ij}}{\lambda_d}\right) \mathbf{r}_{ij}}{r_{ij}^3 \exp[r_{ij}/\lambda_d]} \tag{4}$$

Also, ω is the rotational rate of the reference (CM) orbit (and the $\mathcal{H}$ frame), $r_{ij} = \|\mathbf{r}_i - \mathbf{r}_j\|$ is a separation distance between crafts i and j, and x, y, and z denote components along the axes $\hat{e}_R$, $\hat{e}_T$, and $\hat{e}_N$, respectively. The adopted Coulomb force model provides conservative accounting of plasma shielding, and is demonstrated to be highly accurate in GEO, both experimentally and numerically, for $r_{ij} > 10R_{sc}$ [30,17]. Therefore, formations in the GEO regime with r_{ij} bounded from below, and a constant and nominal λ_d value are assumed.

2.2. Hill-frame constant of motion

Consider a Coulomb formation of N craft, using the Fig. 1 notation, and Eq. (4) dynamics. Norman and Peck [34] demonstrate that mechanical energy and total angular momentum are conserved, in systems acted on by central body gravity and conservative internal forces. Coulomb forces are not generally conservative, but those considered in this work are because, although time-varying, they depend only on generalized coordinates (i.e. time-varying craft positions). Nevertheless, Hussein and Schaub [14,10] and Schaub and Kim [20] show, in general, that Coulomb forces cannot alter a system's inertial angular momentum vector, denoted $\mathbf{H}_0$, and defined by

$$\mathbf{H}_0 = \sum_i m_i \left(\mathbf{R}_i \times \frac{^{\mathcal{N}}\mathrm{d}}{\mathrm{d}t} \mathbf{R}_i \right) \tag{5}$$

The $\mathbf{H}_0$ vector can alternatively be written as the sum of two angular momentum terms, as in Eqs. (6a) and (6b). The terms being the momentum $\mathbf{H}_{\mathrm{cm}}$ associated with a total mass $M = \sum_i m_i$ on the CM orbit, and the angular momentum $\mathbf{H}_G$ of the particles moving with respect to the CM. It is important to note that no dynamical simplifications have been made, thus far:

$$\mathbf{H}_0 = M \left(\mathbf{R}_{\mathrm{cm}} \times \frac{^{\mathcal{N}}\mathrm{d}}{\mathrm{d}t} \mathbf{R}_{\mathrm{cm}} \right) + \sum_i m_i \left(\mathbf{r}_i \times \frac{^{\mathcal{N}}\mathrm{d}}{\mathrm{d}t} \mathbf{r}_i \right) \tag{6a}$$

$$\mathbf{H}_0 = \mathbf{H}_{\mathrm{cm}} + \mathbf{H}_G \tag{6b}$$

Inherent to the Hill-Frame definition is the assumption that $\mathbf{H}_{\mathrm{cm}}$ is constant. With this assumption, Eqs. (6a) and (6b) imply that $\mathbf{H}_G$ is constant. Also, the reference orbit $\hat{e}_R$–$\hat{e}_T$ is assumed coplanar to the $\hat{\imath}$–$\hat{\jmath}$ plane (an arbitrary choice). Therefore, $\mathcal{H}$ is obtained by rotating $\mathcal{N}$, about $\hat{k} = \hat{e}_N$, at the constant rate ω (also inherent to the Hill-Frame definition). The angular velocity vector of the $\mathcal{H}$ frame is then: $\boldsymbol{\omega} = \omega\hat{k} = \omega\hat{e}_N$. Next, the $\mathbf{H}_G$ vector, transformed to the rotating Hill-Frame, is denoted $\mathbf{h}_G$. The time-derivative of $\mathbf{h}_G$ taken with respect to the $\mathcal{H}$ frame, is computed in Eq. (7a), via the transport theorem. Also, $\mathbf{h}_G$ is defined component-wise (in the $\mathcal{H}$ basis) by Eq. (7b):

$$\frac{^{\mathcal{H}}\mathrm{d}}{\mathrm{d}t} \mathbf{h}_G = \frac{^{\mathcal{N}}\mathrm{d}}{\mathrm{d}t} \mathbf{H}_G - (\boldsymbol{\omega} \times \mathbf{h}_G) = \begin{bmatrix} 0 \\ 0 \\ 0 \end{bmatrix} - \begin{bmatrix} -\omega h_y \\ \omega h_x \\ 0 \end{bmatrix} \tag{7a}$$

$$^{\mathcal{H}}\mathbf{h}_G = [h_x \; h_y \; h_z]^T \tag{7b}$$

Since $\mathbf{H}_G$ is a constant vector, it is concluded that h_z is a scalar constant of motion, for Hill-Frame formations having internal forces (e.g. Coulomb force). This result is summarized in Eqs. (8a) and (8b), with h_z written in terms of spacecraft coordinates, and its time-derivative taken with respect to the $\mathcal{H}$ frame:

$$h_z = \sum_i m_i (x_i \dot{y}_i - y_i \dot{x}_i) \tag{8a}$$

$$\dot{h}_z = \frac{^{\mathcal{H}}\mathrm{d}}{\mathrm{d}t} h_z = \sum_i m_i (x_i \ddot{y}_i - y_i \ddot{x}_i) = 0 \tag{8b}$$

Position vector time-derivatives $\dot{\mathbf{r}}_i$, taken with respect to the $\mathcal{H}$ frame, are related to the inertial time-derivatives, via the transport theorem, as

$$\dot{\mathbf{r}}_i = \frac{^{\mathcal{H}}\mathrm{d}}{\mathrm{d}t} \mathbf{r}_i = \frac{^{\mathcal{N}}\mathrm{d}}{\mathrm{d}t} \mathbf{r}_i - (\boldsymbol{\omega} \times \mathbf{r}_i) = \begin{bmatrix} \dot{x}_i \\ \dot{y}_i \\ \dot{z}_i \end{bmatrix} \tag{9}$$

2.3. Two-craft Hill-Frame constant of motion

For the special case of two vehicles, Eq. (3) constraint can be used to eliminate one craft's state variables from Eqs. (8a) and (8b). In Eq. (10), the craft 2 state is written in terms of craft 1, with the subscripts on $\mathbf{r}_1$ components omitted, for simplicity:

$$\mathbf{r}_2 = \frac{-m_1}{m_2} \mathbf{r}_1 = \frac{-m_1}{m_2} \begin{bmatrix} x \\ y \\ z \end{bmatrix} \quad \dot{\mathbf{r}}_2 = \frac{-m_1}{m_2} \begin{bmatrix} \dot{x} \\ \dot{y} \\ \dot{z} \end{bmatrix} \tag{10}$$

Upon substitution, the 2-craft integral of motion (and its $\mathcal{H}$ frame derivative) is given by

$$h_z = \frac{m_1^2 + m_1 m_2}{m_2} (x\dot{y} - y\dot{x}) \tag{11a}$$

$$0 = x\ddot{y} - y\ddot{x} \tag{11b}$$

2.4. Reduced and normalized two-craft dynamics

Eq. (10) is substituted into Eq. (4), to explicitly remove $\mathbf{r}_2$ terms from the craft 1 acceleration. Then a scaled charge

product $\tilde{Q}_{12}$, given by Eq. (12), is substituted into the resulting expression. The scaled charge product substitution introduces a time transformation into the equations of motion. This transform to the non-dimensional time-like variable τ, is defined by Eq. (13):

$$\tilde{Q}_{12} = \frac{k_c Q_{12}}{\omega^2} \tag{12}$$

$$d\tau = \omega dt \quad (\zeta)' = \frac{d\zeta}{d\tau} = \frac{1}{\omega}\frac{d\zeta}{dt} \tag{13}$$

This yields Eq. (14a), an expression for the scaled craft 1 acceleration (in the variable τ), as a function of its own position vector $\mathbf{r}_1$, its own scaled velocity vector $\mathbf{v}_1 = \mathbf{r}'_1 = \dot{\mathbf{r}}_1/\omega$, and the scaled charge product $\tilde{Q}_{12}$. Eq. (14a) then provides reduced and normalized equations of motion for the system (craft 2 can be explicitly determined using Eq. (3)). The craft 1 subscript is omitted for simplicity (i.e. $\mathbf{r} = \mathbf{r}_1$), and the terms Ψ and M_{r1} are defined in Eq. (14b):

$$\mathbf{r}'' = \frac{\ddot{\mathbf{r}}}{\omega^2} = \begin{bmatrix} 2y' + 3x \\ -2x' \\ -z \end{bmatrix} + \tilde{Q}_{12}\ \Psi(r) \begin{bmatrix} x \\ y \\ z \end{bmatrix} \tag{14a}$$

$$\Psi(r) = \frac{M_{r1}^2\left(1 + \dfrac{r}{M_{r1}\lambda_d}\right)}{m_1\ r^3 \exp\left[\dfrac{r}{M_{r1}\lambda_d}\right]} \quad M_{r1} = \frac{m_2}{m_1 + m_2} \tag{14b}$$

The scaled charge product $\tilde{Q}_{12}$ and scaled dynamics (in the variable τ), simplify the subsequent analysis and numerical integration of periodic Coulomb formations. However, the dimensional electric potential ϕ (in Volts) is often more informative than $\tilde{Q}_{12}$. The dimensional net charge q_1 and potential ϕ_1 are therefore computed from $\tilde{Q}_{12}$ (where necessary) using

$$q_1 = \omega\sqrt{\frac{|\tilde{Q}_{12}|}{k_c}} \quad \phi_1 = \frac{\omega\sqrt{k_c|\tilde{Q}_{12}|}}{R_{sc}} \tag{15}$$

where Eq. (1) relates q_1 to ϕ_1, equal charge magnitudes ($|q_1| = |q_2|$) are assumed, and a positive q_1 convention is adopted.

2.5. Stability determination of periodic motions

Eqs. (14a) and (14b) are written in Eq. (16) state-space form, with $\mathbf{X}(\tau)$ denoting the full-state vector, and its derivative taken with respect to the rotating Hill-Frame denoted $\mathbf{F} = \mathbf{X}'(\tau)$:

$$\mathbf{X}(\tau) = \begin{bmatrix} \mathbf{r} \\ \mathbf{v} \end{bmatrix} \quad \mathbf{X}'(\tau) = \mathbf{F} = \begin{bmatrix} \mathbf{v} \\ \mathbf{r}'' \end{bmatrix} \tag{16}$$

This 1st order ODE system can be linearized about a periodic solution $\mathbf{X}^*(\tau)$, with non-dimensional time period τ_p. Doing so yields Eq. (17), a linear ODE system in which the state-propagation matrix $\mathbf{A}(\tau)$ governs the dynamics of small state perturbations $\delta\mathbf{X}(\tau)$, from $\mathbf{X}^*(\tau)$. A state-transition matrix $\mathbf{\Phi}(\tau, 0)$ may be found, which maps $\delta\mathbf{X}$ from $0 \to \tau$, as defined in Eq. (18). Also, the state-transition matrix (STM) satisfies the same ODE as $\delta\mathbf{X}$, and thereby has the same state-propagation matrix:

$$\delta\mathbf{X}'(\tau) = \left(\left(\frac{\partial\mathbf{F}}{\partial\mathbf{X}}\right)\Big|_{\mathbf{X}=\mathbf{X}^*}\right)\delta\mathbf{X}(\tau) = \mathbf{A}(\tau)\ \delta\mathbf{X}(\tau) \tag{17}$$

$$\delta\mathbf{X}(\tau) = \mathbf{\Phi}(\tau, 0)\ \delta\mathbf{X}(0) \quad \mathbf{\Phi}' = \mathbf{A}(\tau)\ \mathbf{\Phi} \tag{18}$$

The state-propagation matrix $\mathbf{A}(\tau)$ associated with Eqs. (14a) and (14b) dynamics is derived in Eqs. (19a)–(19c), where $\mathbf{0}$ and $\mathbf{I}$ denote 3x3 zero and identity matrices, respectively:

$$\mathbf{A}(\tau) = \begin{bmatrix} \mathbf{0} & \mathbf{I} \\ \frac{\partial\mathbf{r}''}{\partial\mathbf{r}} & \frac{\partial\mathbf{r}''}{\partial\mathbf{v}} \end{bmatrix} = \begin{bmatrix} \mathbf{0} & \mathbf{I} \\ \mathbf{G} & \mathbf{H} \end{bmatrix} \tag{19a}$$

$$\mathbf{H} = \begin{bmatrix} 0 & 2 & 0 \\ -2 & 0 & 0 \\ 0 & 0 & 0 \end{bmatrix} \tag{19b}$$

$$\mathbf{G}(\tau) = \tilde{Q}_{12}\ \Psi(r)\left[\left(\mathbf{I} - \frac{3\mathbf{r}\mathbf{r}^T}{r^2}\right) - \frac{\mathbf{r}\mathbf{r}^T}{M_{r1}\lambda_d(r + M_{r1}\lambda_d)}\right] \tag{19c}$$

This $\mathbf{A}(\tau)$ matrix has the same form, and the same resulting properties as associated with periodic orbits about libration points in the CRTBP [23]. In particular, $\mathbf{\Phi}^T$ is symplectic according to Eq. (20), for the skew-symmetric matrix $\mathbf{J}$:

$$\mathbf{J}\mathbf{F}^T = -\mathbf{F}\mathbf{J} \qquad \mathbf{\Phi}\mathbf{J}\mathbf{\Phi}^T = \mathbf{J} \qquad \mathbf{J} = \begin{bmatrix} \mathbf{0} & \mathbf{I} \\ -\mathbf{I} & \mathbf{G} \end{bmatrix} \tag{20}$$

The STM propagated for τ_p is called the full-cycle Monodramy matrix. The Floquet multipliers σ, correspond to the eigenvalues of the Monodramy matrix, and are used to access Lyapunov stability of $\mathbf{X}^*(\tau)$. Specifically, the orbit is unstable if any $|\sigma_i| > 1$ (and/or if any repeated $|\sigma_i| = 1$ is not semisimple) [21,22]. Also, since $\mathbf{\Phi}(\tau_p, 0)$ satisfies Eq. (20), it exhibits the following properties [22]:

1. $\det(\Phi) = |\Phi| = \pm 1$
2. At least one Floquet multiplier has modulus of unity: $|\sigma_i| = 1$
3. The σ_i appear in reciprocal pairs (i.e. if σ_i is eigenvalue, then so is $\sigma_j = 1/\sigma_i$)

The latter property entails that a σ_i inside the unit circle, has its pair outside (an unstable mode). The maximum modulus Floquet multiplier, denoted $|\sigma|_{\max}$, is then used as a measure for how strongly unstable a particular $\mathbf{X}^*(\tau)$ solution is, and all stability categories, based on the σ_i, are defined in Table 1. These categories imply that asymptotic stability is impossible for all 2-craft periodic Coulomb formations, and at best such solutions will exhibit boundedness (uniform stability).

Table 1
Stability categories based on periodic Coulomb formation Floquet multipliers.

Category	Lyapunov stability
$\lvert\sigma\rvert_{\max} = 1$	
All repeated $\lvert\sigma_i\rvert = 1$ are semi-simple	Bounded
Any repeated $\lvert\sigma_i\rvert = 1$ is not semi-simple	Unstable
$\lvert\sigma\rvert_{\max} > 1$	Unstable

3. Periodic Coulomb formation motions via assumed solutions

The coupling of x and y in Eqs. (14a) and (14b) excludes periodic solutions having only x, y, x and z, or y and z components. Therefore, there are three possible periodic orbit types: $\hat{e}_R$–$\hat{e}_T$ planar motions (in-orbit-plane), $\hat{e}_N$ axis only (normal to orbit-plane), and 3-dimensional motions. In this research, the spacecraft position components are assumed to take the form of simple harmonic oscillators. Therefore, the presented analyses are specific to these periodic flows, which happen to conserve total mechanical energy. Other periodic motions, having assumed functions described by different finite Fourier series, may exist, but are outside the scope of this work. However, the assumed periodic functions are not arbitrary, because the set of allowed motions is restricted, and some examples of inadmissible candidate functions are shown in Section 3.4. Coulomb forces are not generally conservative since active charge control, at the expense of power consumption, can provide arbitrary potential modulation. The open-loop potential functions considered here are explicitly dependent on spacecraft coordinates, and therefore nonconservative Coulomb forcing is also outside of the current scope.

3.1. In-orbit-plane periodic motions

Dynamic Coulomb formations are derived here using Eqs. (14a) and (14b) $\hat{e}_R$–$\hat{e}_T$ planar equations of motion. It is assumed that $x(\tau)$ and $y(\tau)$ are simple harmonic oscillators, defined by

$$x(\tau) = A_x \cos(\theta\tau) \quad y(\tau) = A_y \sin(\theta\tau) \tag{21}$$

Therefore, oscillations occur about $x = y = 0$, with the initial conditions: $x(0) = A_x$ and $y(0) = 0$. The amplitudes of oscillation are denoted A_x and A_y, and θ is the oscillation frequency, related to the relative orbit period t_p (and non-dimensional period τ_p) via

$$\theta = \left(\frac{2\pi}{\tau_p}\right) = \left(\frac{2\pi}{\omega t_p}\right) \tag{22}$$

The time derivatives of x and y are then also periodic and given explicitly by

$$x'\tau) = -\theta A_x \sin(\theta\tau) \quad x''(\tau) = -\theta^2 x(\tau) \tag{23a}$$

$$y'(\tau) = \theta A_y \cos(\theta\tau) \quad y''(\tau) = -\theta^2 y(\tau) \tag{23b}$$

Eq. (21) and Eqs. (23a) and (23b) are then substituted into Eqs. (14a) and (14b), and the resulting $\hat{e}_R$ and $\hat{e}_T$ acceleration terms are divided by $x(\tau)$ and $y(\tau)$, respectively. Rearranging these expressions such that the Coulomb acceleration terms are on the left hand side, results in Eqs. (24a) and (24b), where $\Psi(r)$ is defined in Eq. (14b):

$$\tilde{Q}_{12}(\tau)\Psi(r) = -\theta^2 - 3 - 2\theta\left(\frac{A_y}{A_x}\right) \tag{24a}$$

$$\tilde{Q}_{12}(\tau)\Psi(r) = -\theta^2 - 2\theta\left(\frac{A_x}{A_y}\right) \tag{24b}$$

Note that the right hand sides of Eqs. (24a) and (24b), must be equal, independent of $\tilde{Q}_{12}(\tau)$. Equating these leads to Eq. (25) quadratic equation:

$$\left(\frac{A_y}{A_x}\right) = \frac{-3 \pm \sqrt{9 + 16\theta^2}}{4\theta} \tag{25}$$

This quadratic has two real solutions for all $\tau_p > 0$, since $\sqrt{9 + 16\theta^2}$ is always real, and also insists that $A_x \neq A_y$, meaning that the resulting trajectory is an ellipse about the CM. By choosing the initial condition $A_x > 0$, the two roots of the quadratic may be categorized as follows:

- *Case A* (*The + root*): Ellipse semi-major axis is A_x, and semi-minor axis is A_y ($|A_x| > |A_y|$).
- *Case B* (*The − root*): Ellipse semi-major axis is $-A_y$, and semi-minor axis is A_x ($|A_x| < |A_y|$).

The necessary $\tilde{Q}_{12}(\tau)$ function is derived from either Eq. (24a) or (24b), with the substitution of Eq. (25). This yields Eq. (26), where $\tilde{Q}_{12}(\tau)$ is an explicit function of $x(\tau)$ and $y(\tau)$, since $r^2(\tau) = x^2(\tau) + y^2(\tau)$:

$$\tilde{Q}_{12}(r(\tau)) = \frac{-1}{\Psi(r)}\left[\theta^2 + 3 + \left(\frac{-3 \pm \sqrt{9 + 16\theta^2}}{2}\right)\right] \tag{26}$$

This $\tilde{Q}_{12}(\tau)$ history produces the assumed periodic motion, and is itself a simple oscillator. However, the oscillations are offset from zero, and with period of $\tau_p/2$. Additionally, when $\tau_p = 2\pi$, t_p is equal to the CM orbital period ($\approx$1 day), and the relative orbit has semi-major axis twice that of semi-minor axis. For case B, $\tau_p = 2\pi$ yields a trivial solution of $\tilde{Q}_{12}(\tau) = 0$. The full set of these periodic Coulomb formation motions, in the $\hat{e}_R$-$\hat{e}_T$ plane, can be generated as follows:

1. Choose A_x, and either Case A or Case B of Eq. (25)
2. Solve A_y via Eq. (25)
3. Propagate the controlled system with $\tilde{Q}_{12}(\tau)$ defined by Eq. (26)

3.2. Normal to orbit-plane periodic motions

Here, $\hat{e}_N$ axis oscillations only are considered (the $\hat{e}_R$–$\hat{e}_T$ dynamics are ignored, since they decouple to 1st order). The $z(\tau)$ motion of craft 1 is assumed to oscillate with amplitude A_z about a non-zero offset of z_0, as defined by Eq. (27). Also, it is assumed that $z_0 > A_z$ to avoid collisions of the two craft:

$$z(\tau) = z_0 + A_z \sin(\theta\tau) \tag{27}$$

Unlike the in-orbit plane motions, A_z and z_0 are unrestricted, with the exception that $z_0 > A_z$. The necessary charge history to enable this motion, derived similarly to what was done in Section 3.1, is given by

$$\tilde{Q}_{12}(z(\tau)) = \frac{1}{\Psi(r)}\left[1 - \theta^2 + \theta^2\frac{z_0}{z(\tau)}\right] \tag{28}$$

3.3. Three-dimensional periodic motions

If x, y, and z are assumed to be, τ_p periodic, simple oscillators, the only possible solution is the trivial case of $\tilde{Q}_{12}(\tau) = 0$. However, if $x(\tau)$ and $y(\tau)$ are defined as in Eq. (21), and $z(\tau)$ is defined as in Eq. (29), non-trivial 3D

periodic motions are admitted:

$$z(\tau) = A_z \sin(B_z \theta \tau) \quad B_z = \ldots \frac{1}{8}, \frac{1}{4}, \frac{1}{2}, 2, 4, 8 \ldots \tag{29}$$

For fractional B_z, the relative orbits are τ_p/B_z periodic (with $1/B_z$ planar oscillations in a full period). Whereas for integer B_z, the relative orbits are τ_p periodic (with B_z z-oscillations in a period). Substituting the assumed solutions (and their derivatives) into Eqs. (14a) and (14b), and rearranging, leads to Eq. (30), which provides constraints on the assumed solution parameters. Eq. (31) follows from Eq. (30), upon the substitution of Eq. (25) for the ratio A_x/A_y:

$$\tilde{Q}_{12}(\tau)\Psi(r) = (1 - B_z^2\theta^2) = -\theta^2 - 3 - 2\theta\left(\frac{A_y}{A_x}\right) \tag{30}$$

$$(1 - B_z^2\theta^2) = -\theta^2 - 2\theta\left(\frac{4\theta}{-3 \pm \sqrt{9 + 16\theta^2}}\right) \tag{31}$$

For these 3D solutions, τ_p is no longer free, but rather must satisfy Eq. (31), for a given B_z. Furthermore, Eq. (31) can be written in the form of Eq. (32), a nonlinear root-finding function, in the variable θ. For integer B_z, there is a unique real-valued θ which satisfies Eq. (32), for each of the two cases, corresponding to Eq. (25). For fractional B_z, Eq. (32) admits no real-valued θ solutions:

$$8\theta^2 + (-3 \pm \sqrt{9 + 16\theta^2})[\theta^2(1 - B_z^2) + 1] = 0 \tag{32}$$

Fig. 2(a) plots Eq. (32) versus θ and integer B_z values, for case B (− root in Eq. (25)), and illustrates the existence of unique θ solutions (similar for case A). In contrast, Fig. 2(b) shows that real θ solutions are not permitted for fractional B_z values (true to both cases A and B). Therefore, 3D

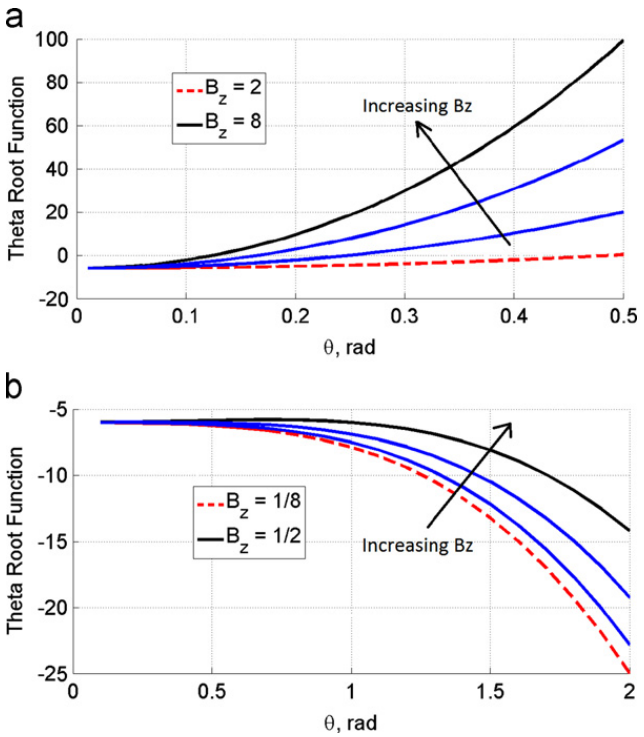

Fig. 2. Three-dimensional periodic solutions: functional relationship between B_z and θ. (a) Case B: Eq. (32) function for integer B_z. (b) Case B: Eq. (32) function for fractional B_z.

periodic Coulomb formations with z-axis oscillations of longer period than planar oscillations, cannot exist. Solutions are limited to the subset of even integer B_z, having $\hat{e}_N$ oscillations that occur B_z times in τ_p. Also, the amplitudes A_x and A_z are free, and so is B_z (in the subset of even integers). This leads to families of 3D, dynamic and periodic, orbits for each case (two roots in Eq. (25)). Orbits within these families can be generated as follows:

1. Choose A_x, A_z, and B_z (even integer)
2. Choose either Case A or Case B of Eq. (25)
3. Solve θ (and τ_p) numerically from Eq. (32)
4. With θ known, solve A_y via Eq. (25)
5. Propagate the controlled system with $\tilde{Q}_{12}(\tau)$ defined by Eq. (26)

3.4. Restrictions on assumed periodic trajectories

Admissible periodic solutions within this model must satisfy Eq. (33), which is the derivative of Eq. (11a) Hill-Frame constant of motion, in terms of the non-dimensional time-variable τ:

$$x(\tau)y''(\tau) - y(\tau)x''(\tau) = 0 \tag{33}$$

This restriction means that $x(\tau)$ and $y(\tau)$ periodic functions cannot be assumed arbitrarily. The following are demonstrable examples of simple periodic functions, which cannot satisfy this condition, and therefore such motions cannot occur.

- *Simple planar harmonic oscillators about the origin:*

$$x(\tau) = A_x \cos(\theta_x \tau) \quad y(\tau) = A_y \sin(\theta_y \tau) \tag{34}$$

Substituting into Eq. (33) yields $\theta_y^2 = \theta_x^2$, then since $\theta > 0$, we find that $\theta_x = \theta_y$. Therefore, Eq. (34) periodic flows having $\theta_x \neq \theta_y$ cannot exist. Hence $\theta_x = \theta_y = \theta$ is used in the previous examples.

- *General rotary motion* (*periodic polar curve*):

$$r(\tau) = A_1 + A_2 \sin(n\theta\tau) \tag{35a}$$

$$x(\tau) = r(\tau)\cos(n\theta\tau) \tag{35b}$$

$$y(\tau) = r(\tau)\sin(n\theta\tau) \tag{35c}$$

where n is a positive integer and $A_2 \neq 0$. Subbing Eqs. (35a)–(35c) into Eq. (33), yields Eq. (36)

$$2nA_2 \cos(n\theta\tau)[A_2 \sin(n\theta\tau) + A_1] = 0 \tag{36}$$

This expression is not true for all τ, and by contradiction, such motions are impossible.

- *Simple planar harmonic oscillators, offset from origin*:

$$x(\tau) = x_0 + A_x \cos(\theta_x \tau) \tag{37a}$$

$$y(\tau) = y_0 + A_y \sin(\theta_y \tau) \tag{37b}$$

If x_0 or y_0 are zero, then Eq. (33) insists that $y(\tau)$ or $x(\tau)$ of Eqs. (37a) and (37b) are constant, both of which are contradictions. For $x_0 \neq 0$, $y_0 \neq 0$, and $\theta_x = \theta_y$ Eq. (33) momenta condition is satisfied. However, it can be readily

Table 2
Numerical test cases: input parameters.

Parameter	Value	Units
a_0	4.227×10^7	m
R_{sc}	1	m
λ_d	180	m
$m_1 = m_2$	150	kg
ω	7.2593×10^{-5}	rad/s
k_c	8.99×10^9	Nm^2 / C^2

shown from the dynamics that no real $Q(\tau)$ history can enable the motion. This shows that Eq. (33) is a necessary (but not sufficient) condition for Coulomb formation periodic orbits, because the assumed trajectory can satisfy Eq. (33), but not the dynamics.

4. Numerical simulations of periodic Coulomb formations

The following results are generated by propagating the dynamical system in Eqs. (14a) and (14b) numerically. The two vehicles are assumed to be of equal radius $R_{sc} = 1$ m. Additional parameter values are listed in Table 2, where a mean λ_d value at GEO is adopted [13].

4.1. In-orbit-plane periodic motions

Example of craft 1 position histories in Figs. 3(a) and (b), and corresponding potential histories in Figs. 4(a) and (b), are shown for A_x=20 m and $\tau_p = \pi$. These provide a comparison of $r(\tau)$ and $\phi_1(\tau)$ between the two cases (A and B).[1]

Note that the ϕ_1 amplitude of oscillation is greater in case A, despite the case B example having a larger energy ellipse. In either case, the ϕ_1 amplitude increases in proportion to A_x, and in inverse proportion to τ_p.

4.2. In-orbit-plane periodic motion stability

Perturbations normal to the orbit-plane decouple from the in-plane dynamics (to 1st order), and the two Floquet multipliers associated with out-of-plane perturbations, have modulus of unity. Values of the remaining four multipliers, or Monodramy matrix eigenvalues, are functions of A_x, τ_p, and case A/B selection. Trends in the magnitude of $|\sigma|_{\max}$, and the real or complex nature of the eigenvalues are summarized as follows:

1. $|\sigma|_{\max} \uparrow$ as $\tau_p \uparrow$ and as $A_x \uparrow$ (weakly for Case A)
2. Case A planar σ_i: 1 purely real pair and 1 complex pair for $\tau_p < 2\pi$ (2 purely real pairs otherwise)
3. Case B planar σ_i: 2 complex pairs for $\tau_p < 2\pi$ (1 purely real pair and 1 complex pair otherwise)

In both cases, $|\sigma|_{\max} \approx 1$ for $\tau_p \ll 2\pi$, and therefore quickly oscillating formations are weakly unstable. In Fig. 5(a) and (b),

[1] In Fig. 3(a) and 4(b) and subsequent figures, S/C is used as a shorthand for spacecraft.

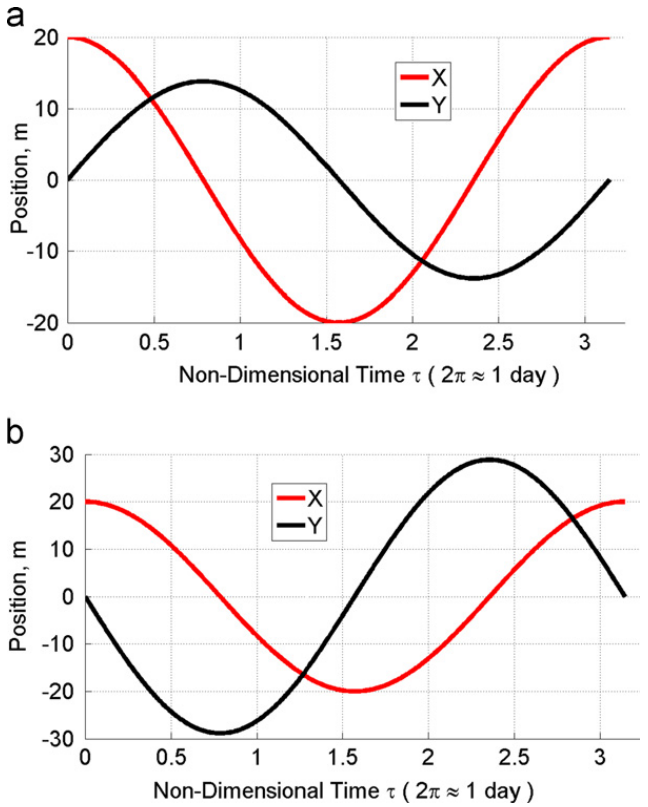

Fig. 3. Planar periodic solution S/C 1 position histories: $A_x = 20$ m, and $\tau_p = \pi$. (a) Case A: $A_x > A_y$. (b) Case B: $A_x < A_y$.

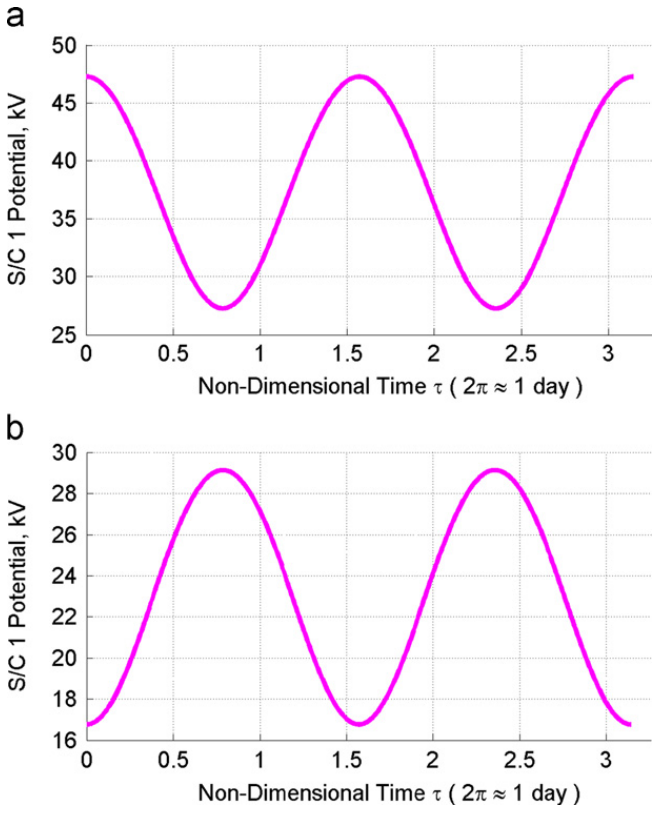

Fig. 4. Planar periodic solution S/C 1 potential histories: A_x=20 m, and $\tau_p = \pi$. (a) Case A: $A_x > A_y$. (b) Case B: $A_x < A_y$.

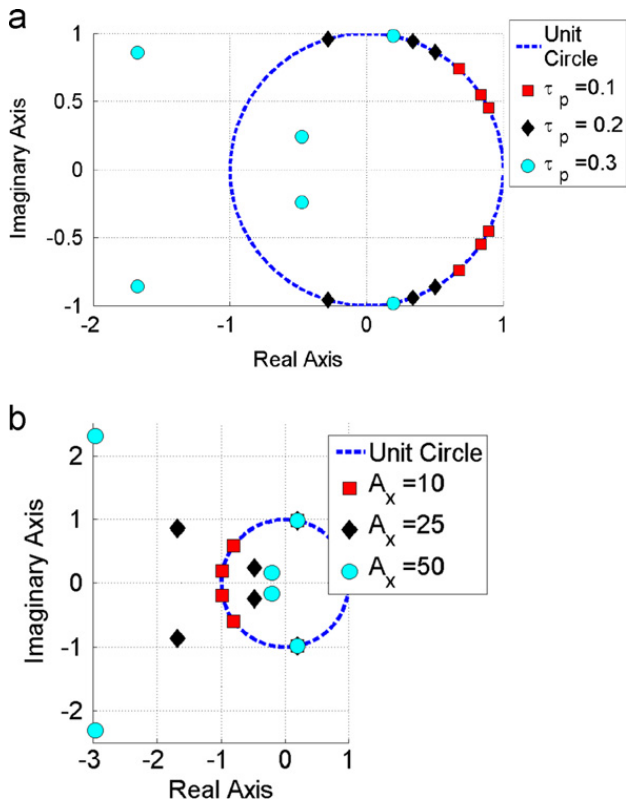

Fig. 5. Case B Floquet multipliers in the complex plane versus: period τ_p and amplitude A_x. (a) Versus τ_p (A_x=25 m). (b) Versus A_x ($\tau_p = 0.3$).

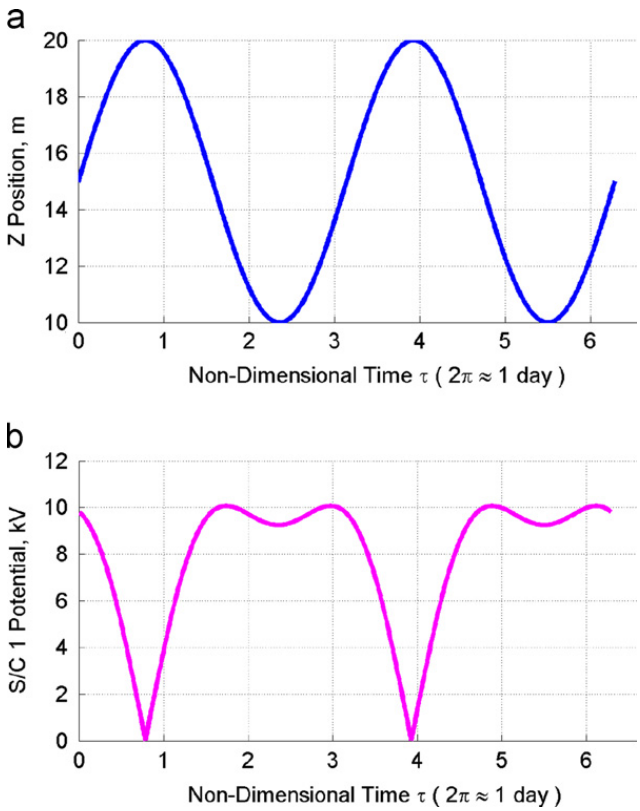

Fig. 6. Normal to orbit-plane solution over two periods: $z_0 = 15$ m, A_z=5 m, and $\tau_p = \pi$. (a) S/C 1 Position History. (b) S/C 1 Potential History.

Monodramy matrix eigenvalues associated with a case B formation are shown in the complex plane, for varying A_x and τ_p. The parameter dependent stability is clear, and it is also evident that two of the σ_i (those associated with $\hat{e}_N$ modes) remain on the unit circle, moving along it as a function of τ_p. These plots demonstrate very near marginal stability for case B formations, having periods on the order of 1 h, and separation distance on the order of tens of meters.

4.3. Normal to orbit-plane periodic motions

An example of orbit-normal oscillatory solution is shown in Figs. 6(a) and (b), propagated for two periods, with $z_0 = 15$ m, A_z=5 m, and $\tau_p = \pi$. Unlike in the planar solutions, $\phi_1(\tau)$ is not a simple harmonic oscillator function. At the maximum separation distance (40 m), the potential goes to zero, and near the minimum separation distance the potential has a dip. This dip is due to the increased Coulomb interaction there, and as the ratio of z_0/A_z increases this dip tends to smooth out.

4.4. Normal to orbit-plane periodic motion stability

Perturbations along the $\hat{e}_N$-axis are marginally stable, but perturbations in the reference orbit plane exhibit unstable and stable modes. The maximum modulus eigenvalue of the Monodramy matrix is a function of z_0, τ_p, and the ratio A_z/z_0 (ratio is between 0 and 1). These functional trends are summarized as follows:

1. $|\sigma|_{\max} \uparrow$ as $A_z/z_0 \uparrow$ (and weakly as $z_0 \uparrow$)
2. $|\sigma|_{\max} \uparrow$ as $\tau_p \uparrow$ (for $0 < \tau_p < \approx 1$ h)
3. $|\sigma|_{\max} \downarrow$ as $\tau_p \uparrow$ (for $\tau_p > \approx 1$ h)
4. Depending on parameters, σ_i may be all complex, all real, or 2 complex pairs and 2 real.

For t_p small (order of minutes) and $A_z/z_0 < 0.1$, $|\sigma|_{\max} \leq 1.0007$ (meaning that very fast, small amplitude, oscillatory motions along the $\hat{e}_N$-axis are weakly unstable).

4.5. Three-dimensional periodic motions

An example of dynamic and periodic Coulomb formation in 3D, is illustrated in Fig. 7(a) and (b), for $A_x > A_y$ (case A), A_x=20 m, A_z=10 m, and B_z=2. The necessary oscillation period (solved numerically) is around 0.73 days. Similar to the $\hat{e}_N$ only oscillatory solution (and unlike the planar solutions), $\phi_1(\tau)$ is not a simple harmonic oscillator. A 3D plot of this trajectory (craft 1) is shown in Fig. 8(a), and the geometry is that of a saddle. Additionally, a different example trajectory is presented in Fig. 8(a), and demonstrates some of the rich geometry found in these orbit families. This latter orbit is of the case B family, and generated with the same A_x and A_z (as case A example), but with B_z=4, and it has a longer period

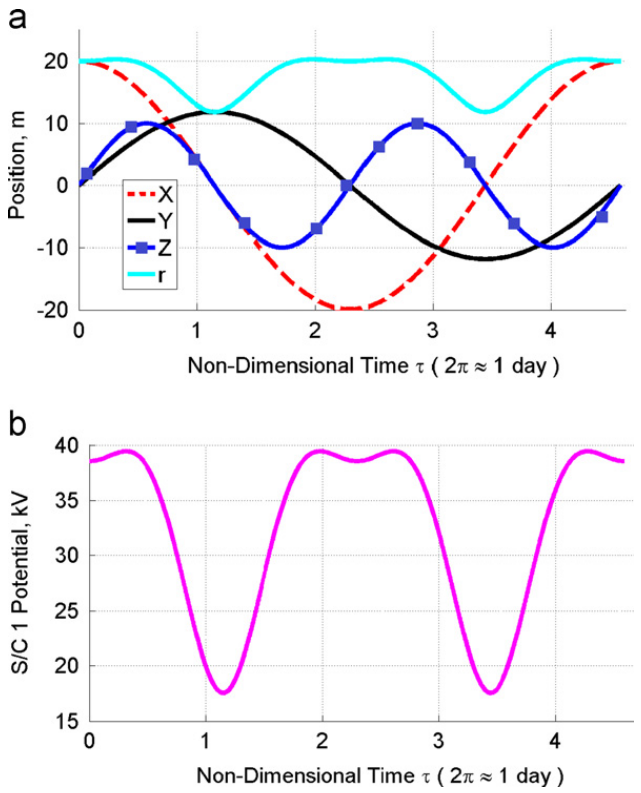

Fig. 7. Three-dimensional (Case A) periodic solution over one period: $A_x=20$ m, $A_z=10$ m, and $B_z=2$. (a) S/C 1 position history. (b) S/C 1 potential history.

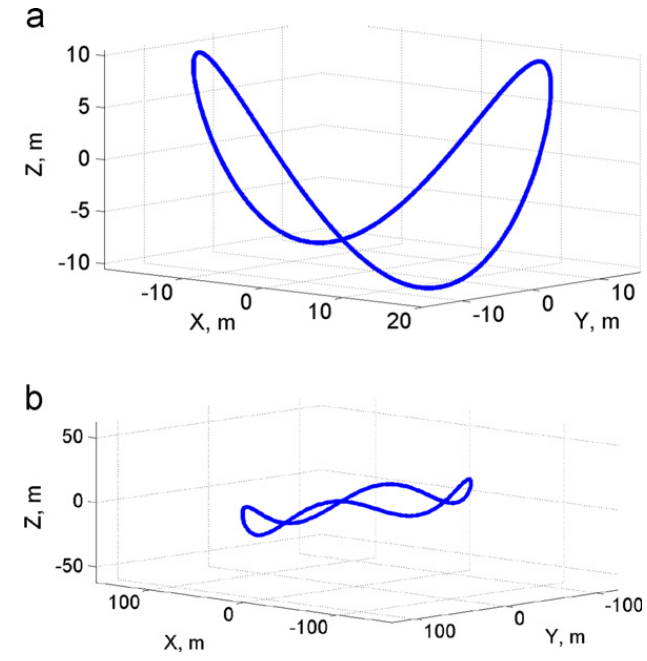

Fig. 8. Three-dimensional periodic solution S/C 1 trajectories: $A_x=20$ m and $A_z=10$ m. (a) Case A trajectory $B_z=2$. (b) Case B Trajectory $B_z=4$.

(≈4.4 days). Some qualitative differences between cases A and B include case B having longer period, and a potential function that exhibits simple harmonic oscillation (unlike that of case A).

4.6. Three-dimensional periodic motion stability

For these orbit families, $|\sigma|_{\max}$ magnitude is a function of: B_z, A_x, A_z, and case A/B selection. The following trends are the result of varying $2\leq B_z\leq 8$, $10\leq A_x\leq 100$ m, and $5\leq A_z\leq 80$ m.

1. Both cases: $|\sigma|_{\max}\uparrow$ as $B_z\uparrow$
2. Case A: $|\sigma|_{\max}\uparrow$ as $|A_x-A_z|\uparrow$ (although this is often weak and/or non-monotonic)
3. Case B: $|\sigma|_{\max}\uparrow$ as $A_x\uparrow$ and as $A_z\downarrow$ (although the latter is often weak and/or non-monotonic)

For both cases, the significant driver of orbit instability is B_z. And generally, case A orbits exhibit $|\sigma|_{\max}$ of much larger magnitude than those associated with case B. The smallest value found for case A orbits is $|\sigma|_{\max}=3511$ ($B_z=2$, $A_x=50$, $A_z=80$). Whereas the case B solutions have $1.8\leq|\sigma|_{\max}\leq 1500$, with $|\sigma|_{\max}=1.8$ occurring at $B_z=2$, $A_x=10$, and $A_z=45$. Again, all are Lyapunov unstable, but the case A solutions tend to be more unstable.

5. Conclusions

The existence of dynamic and periodic Coulomb formations is demonstrated for two spacecraft in a linearized gravity Hill-Frame model. These are the first results of repeating relative orbital motions, where the charge is dynamically varied in an open-loop manner. The results provide a valuable extension to the many works concerning static Coulomb formation solutions (fixed distances and constant potentials). Some possible applications for these nearly propellant-less relative orbits include interferometry with variable separation distance (and the possibility of an inertially fixed line-of-sight vector), Earth/Sun imaging applications, and autonomous inspection of a cooperating or non-cooperating vehicle. Therefore detailed examinations into utilizing these electrostatically forced periodic solutions, should be considered in future research. Also, the derived orbits exhibit varied relative instability, and the implications of this for feedback stabilization should be explored further.

This investigation restricts attention to 2-craft formations with approximate dynamics, and so future research should attempt to derive analogous oscillatory flows for 3-craft (or even N-craft) Coulomb formations, within this dynamical model or otherwise (e.g. nonlinear gravity or CRTBP). Moreover, the examples given here, represent assumed solutions, but not an exhaustive presentation of all possible periodic motions. However, assumed craft position functions are non-arbitrary and the full set of solutions will exist as a subset of the infinite Fourier series representation. Future research should determine the existence of these hypothesized solutions, and the Hill-Frame integral of motion, derived in this work, could facilitate such efforts. Lastly, the sensitivity of all motions to primary perturbations should be analyzed, along with the validity of the restrictions imposed on possible orbits, when considering an increased fidelity force model.

Acknowledgment

This research was made with Government support under and awarded by the Department of Defense (DoD) through the National Defense Science and Engineering Graduate (NDSEG) Fellowship Program.

References

[1] J.H. Cover, W. Knauer, H.A. Maurer, Lightweight reflecting structures utilizing electrostatic inflation, US Patent 3,546,706, 1966.
[2] L. King, C. Parker, S. Deshmukh, J. Chong, Spacecraft formation-flying Using Inter-vehicle Coulomb Forces, Technical Report, NASA Institute for Advanced Concepts, 2002.
[3] L. King, C. Parker, S. Deshmukh, J. Chong, Study of interspacecraft Coulomb forces and implications for formation flying, J. Propul. Power 19 (2003) 497–505.
[4] P. Lawson, J. Dooley, Technology Plan for the Terrestrial Planet Finder Interferometer, Technical Report 05-5, NASA Jet Propulsion Lab, 2005.
[5] E. Mullen, M. Gussenhoven, D. Hardy, Scatha, J. Geophys. Sci. 91 (1986) 1474–1490.
[6] E. Whipple, R. Olsen, Importance of differential charging for controlling both natural and induced vehicle potentials on ats-5 and ats-6, in: Proceedings of the 3rd Spacecraft Charging Technology Conference, pp. 888–893.
[7] C. Escoubet, M. Fehringer, M. Goldstein, The cluster mission, Ann. Geophys. 19 (2001) 1197–1200.
[8] D. Moorer, H. Schaub, Geosynchronous large debris reorbiter: challenges and prospects, in: AAS/AIAA Kyle T. Alfriend Astrodynamics Symposium, 10-311, Monterey, CA.
[9] J. Berryman, H. Schaub, Analytical charge analysis for two- and three-craft Coulomb formations, J. Guidance Control Dyn. 30 (2007) 1701–1710.
[10] I.I. Hussein, H. Schaub, Stability and control of relative equilibria for the three-spacecraft Coulomb tether problem, Acta Astronaut. 65 (2009) 738–754.
[11] E. Hogan, H. Schaub, Collinear invariant shapes for three-craft Coulomb formations, in: AIAA/AAS Astrodynamics Specialists Conference, 10-7954, Toronto, ON.
[12] S. Wang, H. Schaub, Nonlinear charge control for a collinear fixed shape, in: AIAA/AAS Astrodynamics Specialists Conference, 10-7955, Toronto, ON.
[13] R. Inampudi, Two-Craft Coulomb Formation Study About Circular Orbits and Libration Points, Ph.D. Thesis, University of Colorado, 2010.
[14] H. Schaub, I.I. Hussein, Stability and reconfiguration analysis of a circularly spinning two-craft Coulomb tether, IEEE Trans. Aerosp. Electron. Syst. 46 (2010) 1675–1686.
[15] E. Hogan, H. Schaub, Linear stability and shape analysis of spinning three-craft Coulomb formations, Celestial Mech. Dyn. Astron. 112 (2012) 131–148.
[16] J. Berryman, H. Schaub, Static equilibrium configurations in geo Coulomb spacecraft formations, in: AAS/AIAA Space Flight Mechanics Meeting, 05-104, Copper Mountain, CO.
[17] A. Natarajan, A Study of Dynamics and Stability of Two-Craft Coulomb Tether Formations, Ph.D. Thesis, Virginia Polytechnic Institute and State University, 2007.
[18] A. Natarajan, H. Schaub, Linear dynamics and stability analysis of a two-craft Coulomb tether formation, J. Guidance Control Dyn. 29 (2006) 831–838.
[19] D. R. Jones, H. Schaub, Collinear three-craft Coulomb formation stability analysis and control, in: AIAA/AAS Astrodynamics Specialists Conference, 12-4721, Minneapolis, MN.
[20] H. Schaub, M. Kim, Orbit element difference constraints for Coulomb satellite formations, in: AIAA/AAS Astrodynamics Specialists Conference, 04-5213.
[21] G. Floquet, Sur les équations différentielles linéaires á coefficients périodiques, Ann. l'École Norm. Supér. 12 (1883) 47–88.
[22] L. Meirovitch, Methods of Analytical Dynamics, McGraw-Hill, 1970.
[23] V. Szebehely, Theory of Orbits: The Restricted Problem of Three Bodies, Academic Press, New York, 1967.
[24] A. Natarajan, H. Schaub, Hybrid control of orbit-normal and along-track two-craft Coulomb tethers, in: AAS/AIAA Space Flight Mechanics Meeting, 07-193.
[25] S. Wang, H. Schaub, One-dimensional 3-craft Coulomb structure control, in: 7th International Conference on Dynamics and Control of Systems and Structures in Space, Greenwich, London, England.
[26] P. Jasch, E. Hogan, H. Schaub, Stability analysis and out-of-plane control of collinear spinning three-craft Coulomb formations, in: AAS/AIAA Spaceflight Mechanics Meeting, 12-151, Charleston, SC.
[27] D.R. Jones, Optimal reconfiguration of Coulomb formations along invariant manifolds, in: AAS/AIAA Spaceflight Mechanics Meeting, 12-104, Charleston, SC.
[28] D.R. Jones, H. Schaub, Optimal reconfigurations of two-craft Coulomb formations along manifolds, Acta Astronaut. 83 (2013) 108–118.
[29] C. Seubert, S. Panosian, H. Schaub, Attitude and power analysis of two-node, multi-tethered Coulomb structures, J. Spacecr. Rockets 48 (2011) 1033–1045.
[30] L. Stiles, C. Seubert, H. Schaub, Effective Coulomb force modeling in a space environment, in: AAS/AIAA Spaceflight Mechanics Meeeting, 12-105, Charleston, SC.
[31] M. Denton, M. Thomsen, H. Korth, S. Lynch, J. Zhang, M. Liemohn, Bulk plasma properties at geosynchronous orbit, J. Geophys. Res. 110 (2005).
[32] W. Clohessy, R. Wiltshire, Terminal guidance system for satellite rendevous, J. Aerosp. Sci. 27 (1960) 653–658.
[33] J. Bittencourt, Fundamentals of Plasma Physics, Springer-Verlag, New York Inc., 2004.
[34] M. Norman, M. Peck, Integrals of motion for planar multi-body, J. Guidance Control Dyn. 34 (2011) 1790–1797.